ARTICLE

Cyclophospholipids Enable a Protocellular Life Cycle

Ö. Duhan Toparlak, Lorenzo Sebastianelli, Veronica Egas Ortuno, Megha Karki, Yanfeng Xing, Jack W. Szostak,* Ramanarayanan Krishnamurthy,* and Sheref S. Mansy*

Read Online

ACCESS | Metrics & More | Article Recommendations | SI Supporting Information

ABSTRACT: There is currently no plausible path for the emergence of a self-replicating protocell, because prevalent formulations of model protocells are built with fatty acid vesicles that cannot withstand the concentrations of Mg^{2+} needed for the function and replication of nucleic acids. Although prebiotic chelates increase the survivability of fatty acid vesicles, the resulting model protocells are incapable of growth and division. Here, we show that protocells made of mixtures of cyclophospholipids and fatty acids can grow and divide in the presence of Mg^{2+}-citrate. Importantly, these protocells retain encapsulated nucleic acids during growth and division, can acquire nucleotides from their surroundings, and are compatible with the nonenzymatic extension of an RNA oligonucleotide, chemistry needed for the replication of a primitive genome. Our work shows that prebiotically plausible mixtures of lipids form protocells that are active under the conditions necessary for the emergence of Darwinian evolution.

KEYWORDS: cyclophospholipids, protocells, artificial cells, prebiotic chemistry, Darwinian evolution
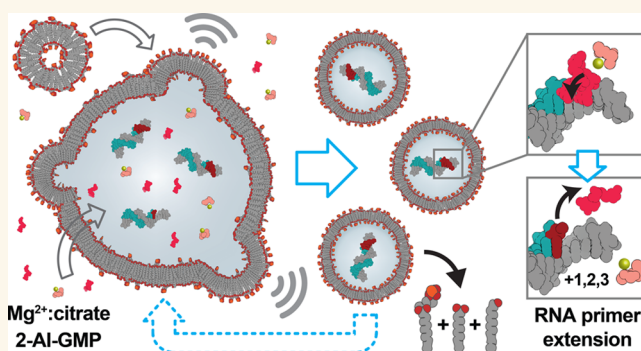
The emergence of Darwinian evolution in populations of protocells depends on the propagation of genetically encoded function, either by enzymatic[1−4] or non-enzymatic[5−7] means. Encapsulation of the genome within lipid vesicles brings several advantages, including protection against parasitic nucleic acid sequences,[8,9] favoring the fitness landscape of nucleic acids,[10−12] and tying nucleic acid chemistry to vesicle growth.[13,14] However, all these benefits presuppose that vesicles can grow and divide in a manner compatible with the replication of encapsulated nucleic acids, i.e., are capable of undergoing a complete protocellular life cycle. While there are many examples of conditions that give rise to the growth and division of fatty acid vesicles in the absence of protein machinery,[13,15−17] none are compatible with known genetic replication mechanisms,[18] despite nearly two decades of investigation.[13,19]

Prebiotically plausible[20] fatty acids are frequently used to construct laboratory models of protocells.[21,22] Their highly dynamic behavior allows for the shape changes needed for growth and division.[15,23,24] The problem is that short-chain, prebiotically plausible fatty acids[25,26] form bilayer membranes that are susceptible to degradation in the presence of free metal ions[27,28] at concentrations necessary for the replication of RNA.[29,30] Stability can be increased through the incorporation of monoglycerides[31,32] or long-chain fatty acids[33,34] into the

membranes of the vesicles, with the presence of amino acids[35] and nucleobases,[36] or the addition of metal ion chelators, such as citrate.[37] However, none of these conditions alone increase protocellular stability sufficiently to be compatible with a complete life cycle. Diacyl phospholipids, as found in biological membranes, form bilayer membranes that are stable enough to be compatible with the conditions necessary for genomic replication,[38,39] even in mixtures with fatty acids.[10,28] However, diacyl phospholipids are not sufficiently dynamic to allow for prebiotically plausible mechanisms of growth and division. Ideally, a lipid that falls in between the two extremes of fatty acids and diacyl phospholipids would give rise to stable vesicles that can also grow and divide.[40,41]

Recently, we showed that a prebiotically plausible derivative of fatty acids, i.e., cyclophospholipids, forms robust vesicles when mixed with short-chain fatty alcohols. Such vesicles can withstand environmentally plausible concentrations of Na^+ and
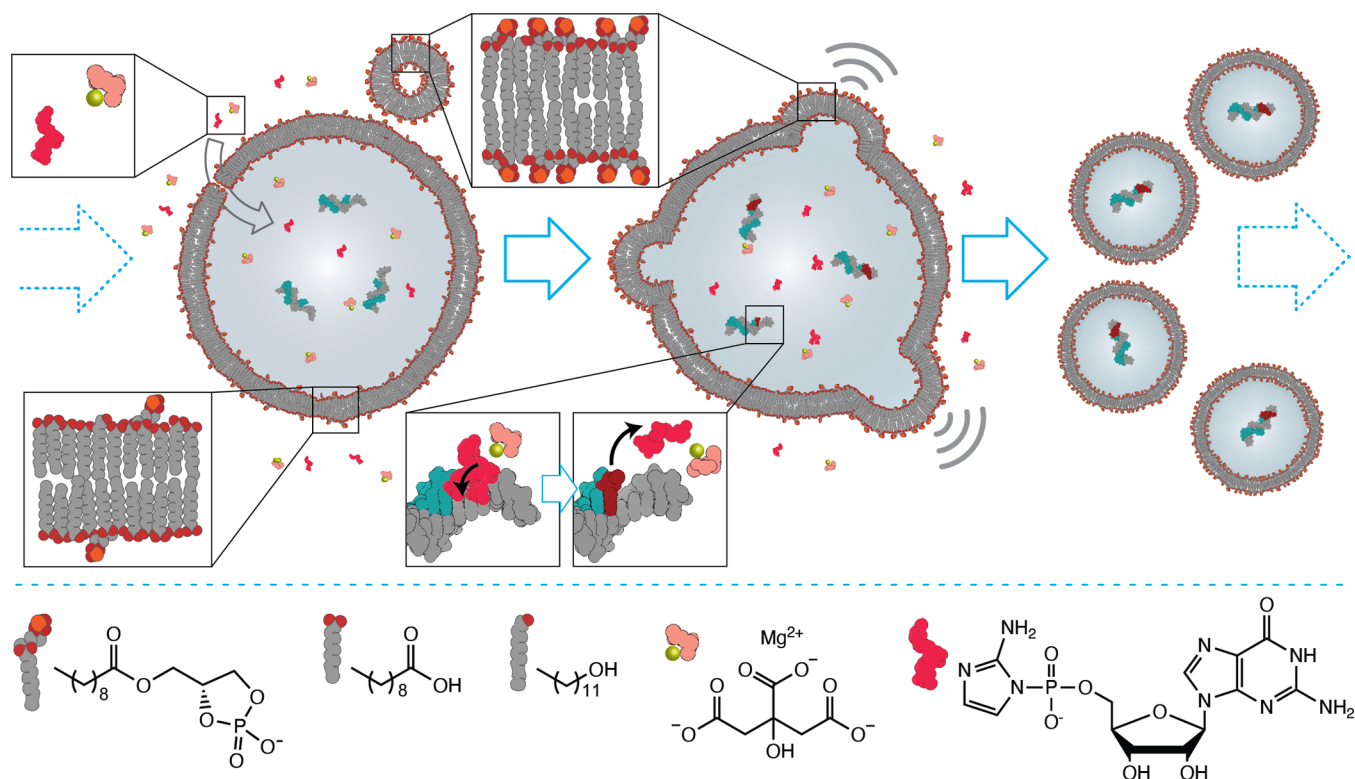
ACS Publications

© 2023 The Authors. Published by
American Chemical Society

23772

https://doi.org/10.1021/acsnano.3c07706
ACS Nano 2023, 17, 23772−23783

Figure 1. Schematic of a protocellular life cycle. Cyclophospholipid vesicles grow through lipid exchange, acquire activated nucleotides (pink) from the environment, copy RNA, bud, and divide, all in the presence of citrate-chelated Mg^{2+} (gold-salmon).

Mg^{2+}.[42] We, therefore, wondered whether these short-chain monoacyl cyclophospholipids would form vesicles with characteristics between those composed of fatty acids and modern-day diacyl phospholipids. That is, in addition to being stable to Mg^{2+}, we sought to determine whether vesicles containing cyclophospholipids were sufficiently dynamic to support growth and division. If so, then protocells possessing a cyclophospholipid membrane could be capable of copying an encapsulated nucleic acid in parallel to growth and division. Here, we show that cyclophospholipids mixed with their precursors, i.e., fatty acids, form stable and dynamic model protocells. This mixed bilayer composition allows the protocells to grow and divide in the presence of citrate chelated Mg^{2+}. Cyclophospholipid protocells acquire activated nucleotides from the environment and are compatible with RNA copying chemistry (Figure 1). Therefore, pathways that led to the phosphorylation of single chain lipids may have given a selective advantage to a subpopulation of protocells that could outcompete their rivals by coupling growth and division with nucleic acid replication.

RESULTS AND DISCUSSION

Cyclophospholipid Vesicles Grow and Divide. To test whether vesicles were capable of growth, vesicles of one composition were fed with vesicles of a different composition of lipid. We previously demonstrated that the mixing of distinct populations of crude, unextruded vesicles composed of fatty acids of different chain-length led to growth due to differences in lipid exchange rates and not due to differences in the size or lamellarity of the vesicles.[17] Large, unextruded multilamellar vesicles (MLVs; ca. 5 μm in diameter) were mixed with smaller, extruded large unilamellar vesicles (LUVs; ca. 100 nm in diameter) to facilitate measurements since LUVs scattered

less light and were not visible by microscopy. In that way, the behavior of one population of vesicles, i.e., the MLVs, could be easily interpreted without interference from the other population of vesicles, i.e., the LUVs. To determine if growth could be achieved by mixing vesicles with different headgroups (cyclophosphate vs carboxylate) as opposed to different lengths of the hydrophobic tails, MLVs and LUVs of different headgroup composition were mixed, e.g., 9:1 cyclophospholipid:fatty acid vesicles mixed with 1:9 cyclophospholipid:fatty acid vesicles and vice versa. The lipid composition of each population of vesicles was chosen to maximize differences in composition and not to maximize stability.

Experiments were run in the presence of 25 mM Mg^{2+}-citrate at pH 8.0; conditions conducive to the nonenzymatic polymerization of nucleic acids[18] but not with the growth and division of fatty acid vesicles lacking cyclophospholipid. Multilamellarity was previously shown to be required for one mechanism of growth and division, which proceeds through filamentous intermediates due to osmotic gradients across the membranes.[15] Vesicle growth was monitored by fluorescence microscopy and by a Förster resonance energy transfer (FRET)-based assay.[17,43] The cyclophospholipids used in this study were either CPC18 or CPC10, which consisted of a monoacylglycerol derived from either oleic acid (C18:1) or decanoic acid (C10:0), respectively, with a cyclic phosphate headgroup (Figure 1 and Figure S1). Oleate, oleyl alcohol, and CPC18 were used to screen conditions and to decipher mechanisms, because of their increased stability and slower dynamics. Subsequently, smaller, prebiotically plausible derivatives of decanoic acid were investigated.

Cyclophospholipid-rich multilamellar vesicles grew when fed with large unilamellar vesicles containing a higher concentration of fatty acid (Figure 2A,C and Video 1). Consistent
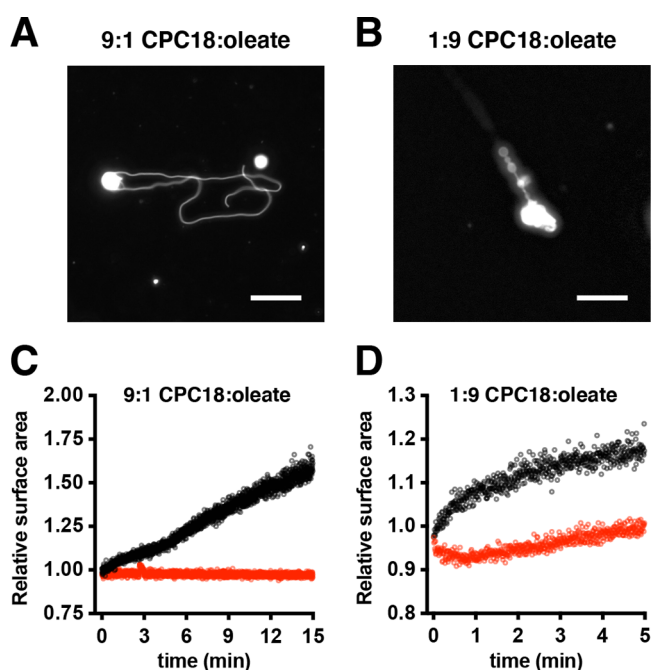
Figure 2. Growth of cyclophospholipid vesicles in the presence of Mg^{2+}-citrate. (A, C) Growth of 9:1 CPC18:oleate MLVs fed with 50 equiv (A) or 25 equiv (C) of 1:9 CPC18:oleate LUVs. (B, D) Growth of 1:9 CPC18:oleate MLVs fed with 5 equiv of pure CPC18 (B) or 25 equiv of 9:1 CPC18:oleate (D) LUVs. Reactions were monitored by epifluorescence microscopy with receiver vesicles labeled with 0.15 mol % LR-DHPE (A, B) and fluorescence spectrophotometry with receiver vesicles containing lipids labeled with FRET donor and acceptor fluorophores (C, D). Red data points represent receiver and donor vesicles of the same lipid composition and black indicates feeding with LUVs of different composition, i.e., 1:9 CPC18:oleate (C) and 9:1 CPC18:oleate (D). Reactions were in 25 mM Mg^{2+}-citrate, 0.2 M Na^{+}-HEPES, pH 8.0. Scale bars are 20 μm.

with prior studies on fatty acid vesicles,[16,44] the spherical multilamellar vesicles transformed into filamentous structures during growth. For example, 9:1 CPC18:oleyl alcohol and 9:1 CPC18:oleate MLVs grew protrusions upon the addition of excess 1:9 or 1:1 CPC18:oleate LUVs within 15−30 min (Figure 2A and Figure S2). The surface area of 9:1 CPC18:oleate MLVs increased by more than 50% when fed with excess 1:9 CPC18:oleate LUVs (Figure 2C). Cyclophospholipid-based vesicles grew both in the presence and in the absence of 25 mM Mg^{2+}-citrate (Figures S2 and S3). In contrast, fatty acid vesicles lacking cyclophospholipid did not grow in the presence of 25 mM Mg^{2+}-citrate, regardless of whether feeding was with LUVs or micelles (Figure S4). Similar to what was previously observed with the addition of oleate LUVs to myristoleate MLVs,[17] the addition of cyclophospholipid-rich LUVs to cyclophospholipid-deficient MLVs led to less pronounced morphological changes by fluorescence microscopy (Figure 2B). Nevertheless, growth was observed by FRET when 1:9 CPC18:oleate MLVs were fed with 9:1 CPC18:oleate LUVs (Figure 2D). Growth was not observed when the MLVs and LUVs possessed an equivalent composition of lipids, both in the presence and absence of 25 mM Mg^{2+}-citrate (Figure S5). Since both cyclophospholipid-rich and cyclophospholipid-deficient vesicles could grow, the data suggested that if the vesicles were capable of division, then continuous cycles of coupled growth and division could take place within the same environment.

Cyclophospholipid-rich multilamellar vesicles divided when fed with vesicles containing a higher concentration of fatty acid. Budding-off events were observed when either 1:1 CPC18:oleate or pure oleate LUVs were added to 9:1 CPC18:oleyl alcohol MLVs (Figure 3A, Figure S6A, and Video 2). Vesicle counting showed a 2- to 3-fold increase in the number of offspring vesicles (Figure 3B and Figure S6). Just as growth was observed in both directions, the division of cyclophospholipid-deficient MLVs was also prevalent when fed with cyclophospholipid-rich LUVs. When 1:9 CPC18:oleate
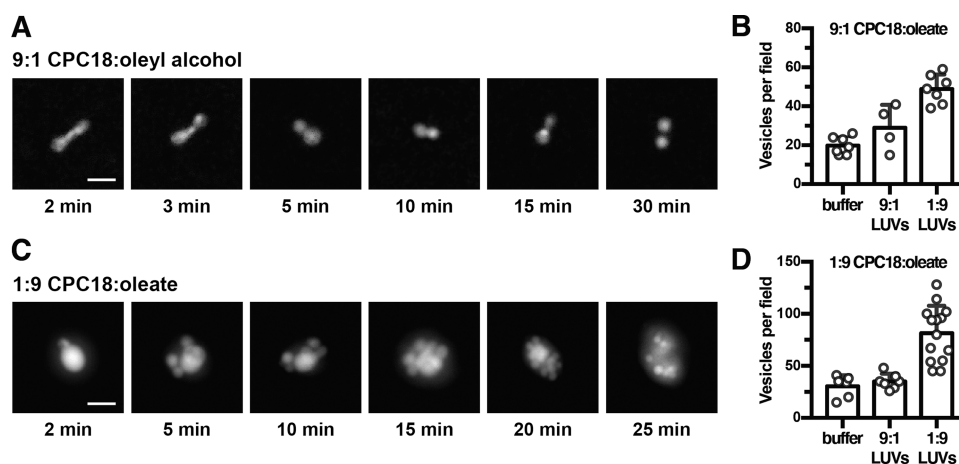
Figure 3. Division of cyclophospholipid vesicles in the presence of Mg^{2+}-citrate. (A) Time-lapse images of vesicle division of cyclophospholipid-rich MLVs (9:1 CPC18:oleyl alcohol MLVs) fed with 50 equiv of 1:1 CPC18:oleate LUVs. (B) The bar graph represents the number of vesicles observed when 9:1 CPC18:oleate MLVs were fed with either 9:1 or 1:9 CPC18:oleate LUVs. (C) Time-lapse imaging of vesicle division of 1:9 CPC18:oleate MLVs fed with 5 equiv. pure CPC18 LUVs. (D) The bar graph represents the number of vesicles observed when 1:9 CPC18:oleate MLVs were fed with either 1:9 or 9:1 CPC18:oleate LUVs. Conditions were 25 mM Mg^{2+}-citrate, 0.2 M HEPES, pH 8.0. Error bars indicate the ± SD of the mean from $n \geq 4$ fields in $n \geq 2$ independent experiments. Scale bars are 10 μm. Vesicles were labeled with 0.15 mol % LR-DHPE.
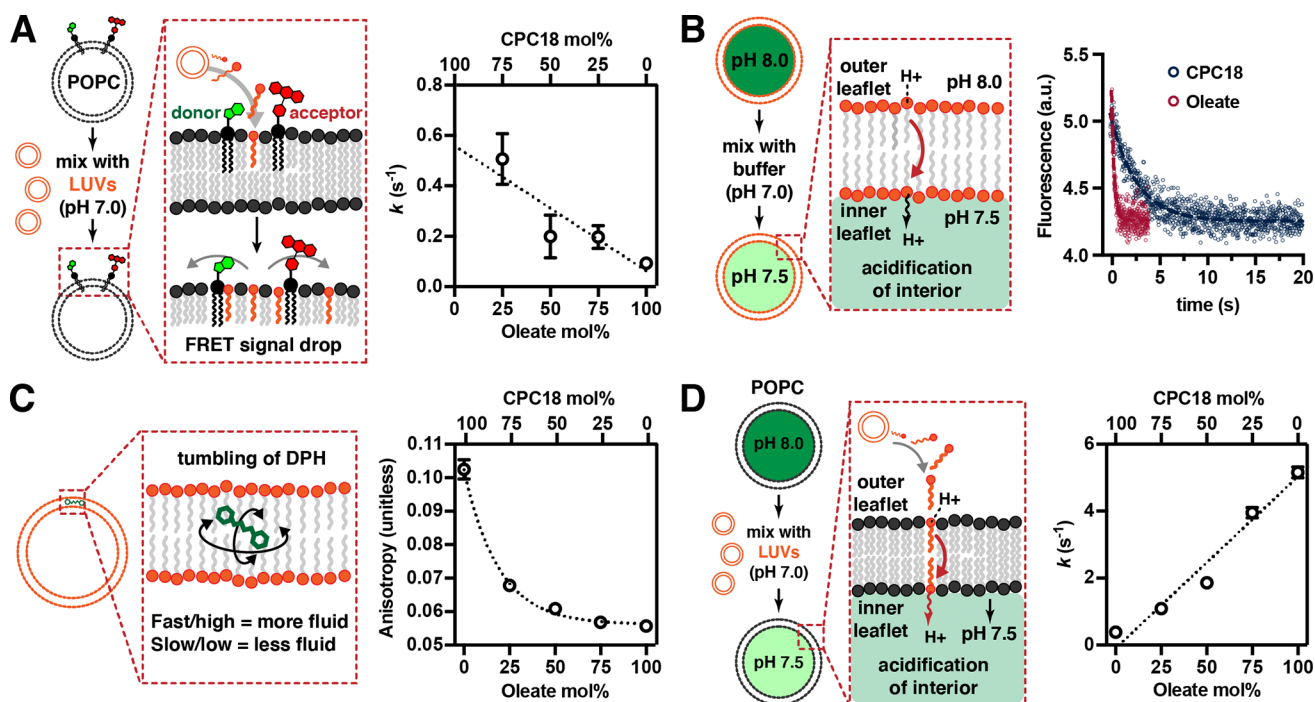
Figure 4. Membrane heterogeneity and monomer kinetics drive the growth and division of protocells. (A) Determination of the lipid exchange rates between vesicles containing oleate and CPC18 with FRET-labeled POPC vesicles. Data were linearly fit with a $R^2 = 0.8$. (B) Flip-flop rates of oleate and CPC18. Representative stopped-flow kinetic data showing the decay of a pH gradient across the membranes of oleate and CPC18 LUVs. Data were fit to a one-phase exponential decay with $R^2 > 0.82$. (C) Determination of the fluidity of membranes with varying ratios of oleate and CPC18. Data are of the fluorescence anisotropy of the hydrophobic reporter molecule 1,6-diphenyl-1,3,5-hexatriene (DPH). Data were fit to a one-phase exponential decay with $R^2 = 0.99$. (D) Acidification of POPC vesicles upon mixing with vesicles containing different ratios of oleate and CPC18. Data were linearly fit with $R^2 = 0.96$. Experiments were performed in 0.2 M Na$^+$-HEPES, pH 8.0.

MLVs were fed with pure CPC18 LUVs, the number of offspring vesicles increased over 25 min (Figure 3C,D and Video 3). The division of 1:9 CPC18:oleate MLVs led to two- to 3-fold increase in the population of offspring vesicles when fed with 9:1 CPC18:oleate LUVs (Figure 3D and Figures S6 and S7) and a 20- to 100-fold increase when fed with pure CPC18 LUVs (Figures S6E and S8). Although division proceeded in the presence of Mg^{2+}-citrate, division was more pronounced in the absence of Mg^{2+}-citrate (Figure S8). Division may have proceeded through different mechanisms, as cyclophospholipid-rich vesicles and cyclophospholipid-deficient vesicles showed different morphological changes during growth. Although it is possible that some fraction of the offspring from cyclophospholipid-deficient vesicles may have been due to the release of internal vesicles after rupture of the exterior membrane, such contributions were likely to have been limited, as judged by the high retention of entrapped material during division, as discussed below. Notably, the division of protocells was not observed when the MLVs and LUVs contained the same molar ratio of lipid (Figures S6–S9). What was critically important for division was a difference in the lipid composition between the receiver and feeder vesicles.

Growth and Division Rely on Differences in Lipid Dynamics. We previously described how the mixing of vesicles composed of fatty acids that were sufficiently different in length led to growth and division.[17] Growth was driven by the disequilibria of lipid concentrations between membranes that possessed low energetic barriers to lipid exchange. The morphological changes that accompanied division were

possible because different chain length lipids exchanged between membranes and flipped between leaflets of the same membrane at different rates. Such kinetic disparities led to imbalances between surface area and volume during growth that led to the shape changes that enabled division.[17,45,46] Similar effects have been proposed to occur due to differences in the hydrophilic headgroup as opposed to the hydrophobic tail of the lipid.[47] We, therefore, tested the hypothesis that lipids with either a cyclophosphate headgroup or a carboxylate headgroup would display kinetic differences that would explain the observed growth and division.

First, the desorption rate of lipids from unlabeled donor vesicles was quantified by mixing with FRET-labeled acceptor POPC (1-palmitoyl-2-oleoyl-sn-glycero-3-phosphocholine) vesicles (Figure 4A). Since the entry of free lipids into vesicles was diffusion limited,[48] decreased FRET efficiencies of the acceptor vesicles reflected the rate of desorption from the donor vesicles. The rate of desorption was positively correlated to the mole fraction of CPC18. For example, the rate of lipid desorption was more than 2-fold greater for 3:1 CPC18:oleate than for 1:3 CPC18:oleate. The data were consistent with the increased hydrophilicity of CPC18 with respect to oleate (Figure S10A).[49] To confirm the fast exchange kinetics of CPC18, FRET-labeled pure CPC18 vesicles were mixed at equimolar concentrations with unlabeled oleate vesicles with different mole fractions of CPC18. As expected, the FRET-labeled CPC18 vesicles initially lost lipid because of the increased desorption rate of CPC18 with respect to oleate (Figure S11A). When the difference in concentration of oleate between the two populations of vesicles was much larger than
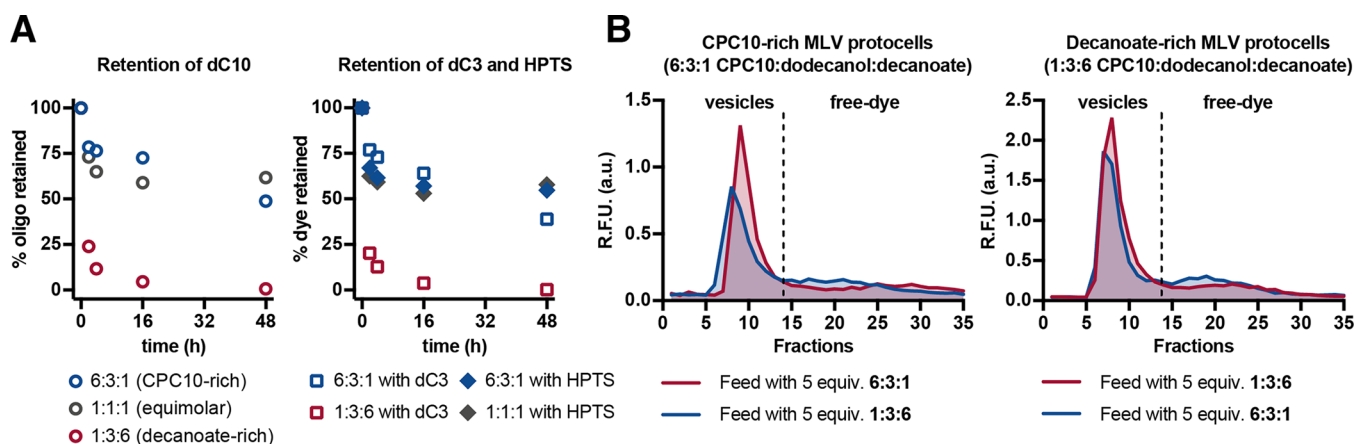
Figure 5. Cyclophospholipid protocells retain oligonucleotides during growth and division in the presence of Mg^{2+}-citrate. (A) Stability of protocells and leakage of molecules across the bilayers of 6:3:1, 1:1:1, and 1:3:6 CPC10:dodecanol:decanoate vesicles. (B) Stability of multilamellar vesicular protocells with membrane composition of (left) 6:3:1 CPC10:dodecanol:decanoate (CPC10-rich) and (right) 1:3:6 CPC10:dodecanol:decanoate (decanoate-rich). The protocells were fed with 5 equiv. LUVs. All data was collected in 25 mM Mg^{2+}-citrate, 0.2 M Na^+-HEPES, pH 8.0. The protocells contained 10 μM entrapped 6-FAM-labeled 10-mer DNA.

that of CPC18 (e.g., when pure CPC18 was mixed with 9:1 CPC18:oleate), CPC18 vesicle growth, due to the equilibration of oleate, was observed after an initial loss of CPC18 (Figure S12A). This two-phase process was more prominent when a 5-fold molar excess of pure oleate vesicles was added to pure CPC18 vesicles (Figure S12B). Conversely, if the FRET-labels were placed in oleate vesicles instead of CPC18 vesicles, the surface area of the oleate vesicles was observed to rapidly increase upon mixing, consistent with the increased dynamics of CPC18 (Figures S11B and S12). Here again, two-phase processes were observed but with growth, owing to the influx of CPC18, occurring first followed by lipid loss, due to the equilibration of oleate (Figure S12). Importantly, since none of the lipids were kinetically trapped within vesicles, the excesses of one population always led to the growth of the vesicles present at lower concentration, as we previously described for mixtures of fatty acid vesicles.[17] Since pure CPC18 forms both micelles and vesicles (Figure S13), unlike solutions containing CPC18 supplemented with oleyl alcohol which only formed vesicles, there may have been multiple mechanisms leading to growth soon after mixing, including a micelle-driven process.[43]

While differences in lipid exchange kinetics between different membranes help to explain growth, these kinetic processes alone are insufficient to explain division. Division requires subspherical volume which leads to shape changes that favor division. To probe whether the surface area increased faster than volume to transiently give rise to subspherical volumes, flip-flop dynamics were measured by monitoring the dissipation of an imposed pH gradient. In contrast to the increased desorption rates of CPC18 discussed above, CPC18 flipped between leaflets of the membrane ca. 10-fold slower than oleate (Figure 4B). Anisotropy measurements of the membrane partitioning fluorophore 1,6-diphenyl-1,3,5-hexatriene (DPH) showed increased rigidity for cyclophospholipid-rich membranes in comparison to fatty-acid-rich membranes, as expected for lipids that flipped less readily (Figure 4C). Slower flip-flop was likely due to the increased size and decreased protonation[42] of the cyclophospholipid headgroup between pH 7 and 8 in comparison to the carboxylate headgroup of oleate. To confirm that lipid flip-flop was limiting during growth, donor vesicles of varying compositions were mixed with reporter POPC vesicles

containing an entrapped pH-sensitive fluorophore. Here, the rate of change in pH encompassed both lipid exchange and flip-flop. Acidification of the lumen was ca. 13 times slower with CPC18 donor vesicles than with oleate donor vesicles (Figure 4D and Figure S14), consistent with the slower flip-flop of the cyclophospholipid. In summary, CPC18 equilibrated between the outer leaflets of membranes of different vesicles faster but equilibrated between leaflets of the same membranes slower than oleate. The differences in dynamics between CPC18 and oleate were similar to previous measurements on fatty acids of different chain length,[17] consistent with division being driven by an influx of lipid to the outer leaflet of the receiver vesicles that outpaced equilibration across leaflets and lamellae. The resulting imbalance in surface area and volume then led to division, although the specific details of the process require further investigation to decipher.

Cyclophospholipid Vesicles Are as Permeable as and More Stable than Oleate Vesicles. Despite slower flip-flop kinetics, pure CPC18 vesicles were more permeable to ribose than pure oleate or POPC vesicles (Figure S15A,B). The addition of 10 mol % oleyl alcohol slightly increased the permeability of CPC18 vesicles, whereas the same concentration, i.e., 10 mol %, of oleate decreased permeability to levels similar to pure oleate vesicles (Figure S15C). The increased permeability of pure CPC18 vesicles may have been due to packing defects that were diminished by the incorporation of oleate. Permeability increased with decreasing pH, consistent with the increased dynamics of protonated lipids (Figure S15D). Importantly, CPC18-containing vesicles were more stable to acidic pH and the presence of Mg^{2+} than oleate vesicles with lower concentrations of CPC18, evaluated by the quantification of released encapsulant (Figures S16 and S17). For example, 1:1 CPC18:oleate vesicles retained more than 50% of encapsulated fluorescein-labeled 10-mer DNA after 72 h at pH 6.0, whereas vesicles with less CPC18, i.e., 1:9 CPC18:oleate, retained less than 25% of the encapsulated oligonucleotide at the same conditions (Figure S17A,B). Similarly, 1:1 CPC18:oleate vesicles retained greater than 75% of the oligonucleotide at pH 8.0 after 24 h in the presence of 7.5 mM Mg^{2+}, whereas only ca. 25% of the DNA oligonucleotide was retained within 1:9 CPC18:oleate vesicles (Figure S17C). The increased stability suggested that cyclo-

phospholipid vesicles may be able to hold nucleic acids throughout a protocellular life cycle, in contrast to protocells solely made of fatty acids.

Cyclophospholipid Protocells Retain Nucleic Acids during Growth and Division. Encouraged by the results obtained with vesicles containing long-chain cyclophospholipids, we next tested whether lipids with prebiotically more plausible, saturated short-chain hydrocarbon tails could also support growth and division. 2:1 CPC10:dodecanol and 6:3:1 CPC10:dodecanol:decanoate multilamellar vesicles (MLVs) formed protrusions when fed with 5 equiv of decanoate-rich (1:3:6 CPC10:dodecanol:decanoate) large unilamellar vesicles (LUVs) in the absence (Figure S18A,C) and presence of 25 mM Mg^{2+}-citrate (Figure S19A). Growth was corroborated by FRET (Figure S18D). CPC10-deficient MLVs also grew and divided when fed with CPC10-rich LUVs, both in the absence (Figure S18E) and presence of Mg^{2+}-citrate (Figure S19C). No growth or division was observed when vesicles were fed with the same composition (Figures S18B,D,F and S19B,D). Taken together, prebiotically plausible mixtures of lipids were capable of growth and division at the concentrations of Mg^{2+} necessary for the replication of nucleic acids. The data suggested that primitive replication cycles of cyclophospholipid-containing protocells could have been supported if the compartments were sufficiently stable to retain their inner contents during growth and division.

To evaluate the stability of prebiotically plausible mixtures of cyclophospholipid containing vesicles, the retention of the negatively charged small molecule fluorophore 8-hydroxypyrene-1,3,6-trisulfonic acid (HPTS) and fluorescein-labeled 3-mer and 10-mer DNA oligonucleotides was tested. The inner contents of 6:3:1, 1:1:1, and 1:3:6 CPC10:dodecanol:decanoate vesicles were quantified by size-exclusion chromatography in the presence of 25 mM Mg^{2+}-citrate (Figure S16). 6:3:1 and 1:1:1 CPC10:dodecanol:decanoate protocells retained ca. 50% of the entrapped molecules after incubation for 48 h (Figure 5A and Figure S20A,C). Similar losses of HPTS and 3-mer and 10-mer DNA indicated that release was due to large-scale rupture of the protocells, as opposed to leakage. Protocells with low cyclophospholipid content, e.g., 1:3:6 CPC10:dodecanol:decanoate, lost nearly all of the encapsulant after 48 h (Figure 5A and Figure S20B). However, the time needed for a single cycle of growth and division was under 10 min and thus much less than the tested 48 h. Shorter times led to increased retention, with 1:1:1 CPC10:dodecanol:decanoate protocells holding more than 75% of the encapsulant for 2 h. Therefore, the data suggested that CPC10-containing protocells may be capable of holding entrapped nucleic acids throughout multiple cycles of growth and division.

Since mixtures of cyclophospholipids and fatty acids gave rise to vesicles that grew and divided and could hold nucleic acids, we next evaluated if protocells built with the same membrane composition could retain nucleic acids during growth and division. Fluorescein-labeled 10-mer DNA was encapsulated within either cyclophospholipid-rich (6:3:1 CPC10:dodecanol:decanoate) or cyclophospholipid-deficient (1:3:6 CPC10:dodecanol:decanoate) protocells. Subsequently, the protocells were fed with 5 equiv of LUVs (1:3:6 CPC10:dodecanol:decanoate and 6:3:1 CPC10:dodecanol:decanoate, respectively) in the presence of 25 mM Mg^{2+}-citrate. Loss of DNA was biphasic with an initial fast phase, which may have been due to osmotic shock followed by much slower

leakage. Nevertheless, more than 75% of the encapsulated DNA was retained after growth and division (Figure 5B). When compared to the loss of material from protocells that were not subjected to growth and division, the process of growth and division only led to the loss of an additional ca. 10% of the DNA from cyclophospholipid-rich and ca. 15% from cyclophospholipid-deficient protocells. Retention of DNA was greater for cyclophospholipid-rich than for cyclophospholipid-deficient vesicles (Figure 5A), suggesting that cyclophospholipid-based protocells better preserved their bilayer integrity during growth and division. Collectively, the data indicated that cyclophospholipids could have facilitated the emergence of chemical systems capable of Darwinian evolution.

Cyclophospholipid Protocells Are Compatible with Nonenzymatic RNA Copying. A minimal system capable of Darwinian evolution could be envisaged as consisting of growing and dividing vesicles that contain a replicating RNA genome. Although such a protocellular system is frequently thought of in terms of an encapsulated ribozyme with RNA polymerase activity,[19] more ancient protocells may have relied on nonenzymatic, template-directed synthesis of an RNA genome.[50] In one strategy, protocells could use nucleotide monophosphates activated with a 2-aminoimidazole at the 5′-position (2-AI) (Figure 1), since such nucleotides are prebiotically plausible and efficiently polymerize in the presence of citrate-chelated Mg^{2+}.[51,52] To demonstrate whether cyclophospholipid-containing vesicles were compatible with RNA copying chemistry, 2-AI activated guanosine (2-AImpG) was added to the outside of cyclophospholipid-deficient (2:3:5 CPC10:dodecanol:decanoate) and cyclophospholipid-rich (6:3:1 CPC10:dodecanol:decanoate) vesicles with entrapped fluorescein-labeled RNA primer and template in the presence of 25 mM Mg^{2+}-citrate (Figure 6A,B). Under these conditions, extension of the encapsulated primer required permeation of the activated nucleotide across the lipid membrane, which was likely facilitated by the neutralizing effects of Mg^{2+}. To ensure that only reactions occurring inside the vesicles were evaluated, aliquots were subjected to size-exclusion chromatography, and the vesicle containing fraction was loaded on a denaturing polyacrylamide gel. Primer extension inside of both model protocells was clear, demonstrating that in addition to growing and dividing, cyclophospholipid-based vesicles were capable of housing the Mg^{2+}-dependent chemistry needed to synthesize RNA in a template-directed fashion (Figure 6C,D).

CONCLUSIONS

Prior reports on model protocells were of vesicles that were either stable and not dynamic or unstable and dynamic. This has led to the synthesis of protocells that either grow and divide under laboratory conditions incompatible with plausible prebiotic environments or could not grow and divide via prebiotically plausible pathways but could survive a wide variety of environments. Here, we show that protocells built with prebiotically plausible lipids, such as mixtures of cyclophospholipids and fatty acids, occupy a space between these two extremes in both being stable and dynamic. This means that cyclophospholipid-containing protocells can grow and divide in the presence of concentrations of Mg^{2+} required for the folding, function, and replication of nucleic acids. Since the final composition of the offspring protocell membranes reflects the ratio of total lipids in solution at equilibrium,
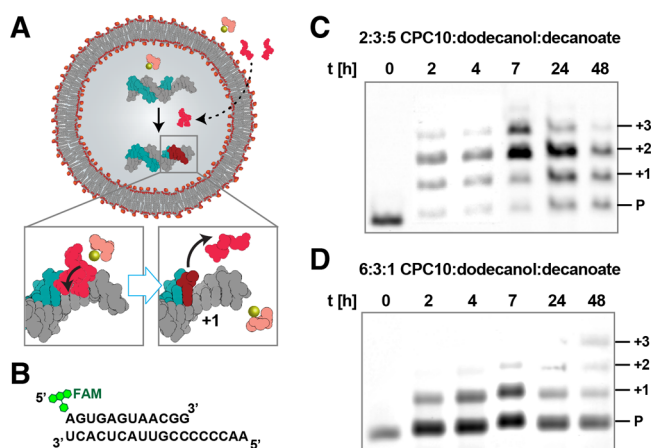
Figure 6. Template-directed, nonenzymatic RNA primer extension within cyclophospholipid protocells. (A) A schematic of the experiment illustrating diffusion of 2-AI activated nucleotide and primer extension. (B) The RNA template and labeled primer encapsulated within the protocell. 2-AImpG was added externally to (C) cyclophospholipid-deficient (2:3:5 CPC10:dodecanol:decanoate) and (D) cyclophospholipid-rich (6:3:1 CPC10:dodecanol:decanoate) protocells. The protocells contained an entrapped fluorescein-labeled RNA primer and an RNA template. Aliquots were removed and purified 0, 2, 4, 7, 24, and 48 h after the addition of the nucleotide and run on a denaturing polyacrylamide gel at approximately the same concentration of RNA. Time zero shows a band corresponding to the primer (P).

multiple rounds of growth and division can be driven by feeding with vesicles of different composition.[17] Potential prebiotic routes for one population of vesicles to encounter another could be the mixing of bodies of water through connecting streams,[53] exchange through aqueous aerosols,[54] or colocalization through convection and thermophoresis.[55] Alternatively, osmotic pressures, potentially resulting from the replication of RNA, could drive the growth of cyclophospholipid-containing protocells.[14]

Cyclophospholipid-containing protocells are sufficiently stable to efficiently retain nucleic acids throughout a complete growth-division lifecycle; therefore, it should now be possible to probe the conditions that mimic the early stages of Darwinian evolution when robust nonenzymatic[6] or ribozyme-based[56,57] replication systems are available. Such a nucleic acid replication system would need to be capable of rapidly reading through complex templates on a time-scale compatible with the kinetics of growth and division and the stability of the vesicles. Once achieved, synergies between lipids and nucleic acids[58] may be uncovered that could not be discerned by working on model protocells and self-replicating RNAs separately. Furthermore, if protein enzymes, such as DNA polymerases or the enzymes required for transcription and translation,[28] are compatible with the cyclophospholipid vesicles, then it should be possible to build selection technologies to investigate evolution[8] and to develop nucleic acids and peptides with sought after function, perhaps aided by microfluidic devices.[59]

The stability of cyclophospholipid vesicles may also facilitate the emergence of metabolic-like chemistry. For example, protometabolic cycles[60,61] using methyl isocyanide activation chemistry[62] and the phosphorylating agent diamidophosphate (DAP)[63] require neutral to acidic conditions which are incompatible with the stability of fatty acid vesicles lacking

cyclophospholipids. Since these activating agents facilitate the synthesis of nucleic acids, peptides, and peptidyl-RNA adducts,[63−65] the increased stability of cyclophospholipid vesicles leads to the increased likelihood of bringing the building blocks of life together. If one of the resulting nucleic acids, for example, possesses the ability to catalyze the synthesis of a cyclophosphate headgroup, then a cascade of reactions leading to the growth and division of the protocell could potentially transpire. Similar schemes were previously proposed for the formation of diacyl phospholipids;[44,66,67] however, the synthesis of cyclophospholipids is simpler than the synthesis of diacyl phospholipids from fatty acids, consistent with increased prebiotic plausibility. Additionally, the dynamics of cyclophospholipids would allow for multiple rounds of growth and division and the uptake of nutrients, all of which are more difficult with diacyl phospholipids.[44] Combined with their stability to environmental concentrations of Na$^+$,[42] cyclophospholipid protocells may also be capable of surviving wet−dry cycling.[68−70] Taken together, the emergence of cyclophospholipids may have served as a useful intermediate between abiotic and biotic chemistry.

METHODS AND EXPERIMENTAL SECTION

Materials and General Experimental. All chemicals were purchased from Merck at the highest possible purity, unless otherwise noted. All organic solvents were purchased as anhydrous (SureSeal) and kept dry. All fatty acids were purchased from Nu-Chek. Fluorescently labeled lipids N-(lissamine rhodamine B sulfonyl)-1,2-dihexadecanoyl-sn-glycero-3-phosphoethanolamine (LR-DHPE) and 1,2-dipalmitoyl-sn-glycero-3-phosphoethanolamine-N-(7-nitro-2-1,3-benzoxadiazol-4-yl) (NBD-PE) were from ThermoFisher Scientific. 1,6-Diphenyl-1,3,5-hexatriene (DPH) was from Acros Organics. 2-(N-Morpholino)ethanesulfonic acid (MES) and 4-(2-hydroxyethyl)-piperazine-1-ethanesulfonic acid (HEPES) were from VWR. 1-[6-(Dimethylamino)naphthalen-2-yl]dodecan-1-one (Laurdan) was obtained from Sigma-Aldrich (Merck). All experiments were performed at room temperature (23 ± 1 °C), unless otherwise noted. pH was measured with a Mettler-Toledo pH meter InLab microtip system. 25 mM Mg^{2+} was provided, when indicated, as a complex with citrate from a stock solution that was prepared at least 1 h in advance. The stock contained 200 mM Mg^{2+} and 800 mM citrate at a 1:4 molar ratio, as previously.[37] NMR spectra were recorded at 298 K using an AV-600 instrument (600 MHz, 500 MHz for ^{1}H and 150 MHz, 125 MHz for ^{13}C). ^{31}P NMR spectra were acquired by using a Bruker DPX-400 instrument. High-resolution mass spectra (HRMS) were obtained on a LCMS TOF mass spectrometer (Agilent ESI-TOF) using electrospray ionization time-of-flight reflectron technique. Microwave reactions were performed using a microwave synthesizer (Initiator Classic, Biotage), in 2−5 mL reaction vials.

Synthesis of Cyclophospholipids. The synthesis of cyclophospholipids followed previous reports.[63,71] Briefly, to a solution of monocaprin (1.0 mmol) or monoolein (1.0 mmol) in 2 mL of N-methyl-2-pyrrolidone (NMP) was added 2−3 mmol of bis-(dimethylamino) phosphorodiamidate (BDMDAP, 2 mmol of CPC10, and 3 mmol of CPC18) and dimethyltin dichloride (C$_2$H$_6$Cl$_2$Sn) (0.2 mmol for CPC10 and 0.3 mmol for CPC18) (Figure S22A). The reaction was subjected to a microwave (120 °C, normal power) for 30 min. A small aliquot of the crude was dissolved in CD$_3$OD to acquire ^{13}C NMR spectra to monitor the reactions. The reactions were stopped when quantitative conversion was observed. The cyclophospholipids were purified through successive liquid−liquid extractions, as previously described (Figure S22A).[71] CPC10 was also synthesized in a single step starting with 2.1 mmol monocaprin as depicted in Figure S21A.[63] For CPC18, Na$^+$ counterions were exchanged with diethylaminoethyl (DEAE) anion exchange chromatography and eluted with 1 M triethylammonium in

water. Concentration by solvent removal via rotary evaporation yielded a yellow oil.

Preparation of Vesicles. The growth and division experiments and the encapsulant retention experiments used 25 mM lipid when oleate and derivatives of oleate were used. When decanoic acid and derivatives of decanoic acid were used, 100 mM lipid was exploited to make the MLVs. All lipid dynamics and ribose permeability measurements were made with 10 mM lipid, unless otherwise noted. All vesicles were prepared by either the hydration of a thin film or dispersion of oil (fatty acids) or powder (cyclophospholipids) in aqueous solution. To generate lipid films, the lipids were first dissolved in HPLC-grade methanol for cyclophospholipids and fatty acids and chloroform for phospholipids. Either 10 mg/mL oleate or 25 mg/mL CPC18 were pipetted into 2 mL HPLC glass vials and the organic solvent evaporated under a stream of N_2 followed by drying under house vacuum overnight (<16 h) to remove the residual solvent. The film was then hydrated with aqueous solution containing fluorescent reporter molecules, vortexed multiple times (each time for 4−5 s), and then tumbled for <24 h. Unilamellar vesicles were prepared by extrusion through 100 nm track-etched polycarbonate membranes with an Avanti miniextruder (≥11 passes). The extruded vesicles were then left undisturbed in the dark overnight (16−24 h) until use. If needed, the vesicles were purified by size exclusion chromatography (SEC) with sepharose 4B. Lipid concentrations were kept above the critical vesicle concentration (CVC) in the running buffer, i.e., 1−2 mM for oleate/CPC18-containing and 20 mM for CPC10-containing vesicles. No extra lipids were added to the running buffer for POPC vesicles. Fractions were collected with either a Gilson FC203 or a Gilson FC204B multichannel fraction collector and analyzed with a Tecan M200 (BioTek) or Varioskan (Thermo-Fisher) plate reader. Fractions containing vesicles were pooled and either used immediately or kept in the dark until use. All purified vesicles were used within 24−72 h of purification. For pH-dependent stability tests, the conditions were as follows: citrate buffer for pH 4.0 and 5.0, MES buffer for pH 6.0, HEPES buffer for pH 7.0 and 8.0, and carbonate/bicarbonate buffer for pH 9.0. Buffers were present at 0.2 M. In all cases, the pH was adjusted either by ratios of the donor and acceptor (citric acid/sodium citrate and carbonate/bicarbonate) or with 5 M NaOH (MES and HEPES). The sodium ion content of all buffers was adjusted with concentrated NaCl to 200 mM.

Microscopy. Vesicles for growth and division experiments either contained encapsulated 5 mM 8-hydroxypyrene-1,3,6-trisulfonic acid (HPTS) or 0.15 mol % LR-DhPE within the membrane. After 24 h of tumbling, the vesicles were extruded through 8 μm track-etched polycarbonate membrane with at least 11 passes (Avanti Polar Lipids). Vesicles with a diameter <5 μm were removed by multiple rounds of brief centrifugation with spin column filters (Ultrafree−MC−Durapore 5 μm with PVDF membrane, Millipore), while keeping the overall lipid concentration at 1 mM with 100 nm extruded vesicles of the same composition. For feeding, 100 nm diameter LUVs were prepared as above and used after equilibration for 24 h. Labeled MLVs were then mixed with 100 nm unilamellar vesicles (without dye) and imaged inside a disposable hemocytometer (Countess, Invitrogen) or single-depression glass slides. For oleate vesicle controls, following preincubation in the dark for 30 min, division was achieved either by firmly pressing onto the hemocytometer or by gently blowing compressed air onto glass slide. For division experiments with CPC18-containing vesicles, no mechanical force was applied apart from initial pipetting. Images were taken on an inverted epifluorescence microscope (Nikon TE2000S or Zeiss Axio Z1 Observer) with extra-long working distance objective lenses. Specifically, the 10× objective was an EC Plan-Neofluar 10×/0.3 Ph1M27, and the 20× objective was a LD Plan Neofluar 20×/0.4 Korr Ph2M27. For Nikon TE2000S, a CCD camera (Hamamatsu) was used for data recording. The exposure time between time-points was fixed at 500 ms (10×) or 250 ms (20×). The vesicles for stability to pH were imaged with a 100× objective (Plan-Apochromat 100×/1.4 oil DIC) or 40× objective (EC Plan Neofluar 40×/0.75), as previously reported.[42] For vesicle counting, random fields were chosen blindly and imaged with constant exposure times, as above. All collected frames/images were then analyzed and processed by Fiji (ImageJ). Vesicle counting was performed manually with Fiji software.

Fluorescence Spectroscopy. Measurements were taken with a QuantaMaster 40 UV−vis spectrofluorometer equipped with two detectors (T-format). For online measurements, quartz cuvettes with a 60 μL final volume and a window z-position of 8 mm were used. The slit openings for the instrument were 0.4−0.5 mm (online measurement) and 1−2 mm (stopped-flow kinetics and MLV measurements). The photomultiplier (PMT) efficiency of the instrument was checked, and amplifier values were adjusted manually using the Raman spectrum of water as a reference. Identical settings were used throughout the studies. Stopped-flow measurements used an attachment from BioTek. For steady-state anisotropy measurements, the slit openings were 0.5 mm. For each individual measurement, the G-factor was calculated for corrections (with preset instrument settings for 1 s) to eliminate errors/variations arising from different detector efficiencies.

Dynamics of Large Unilamellar Vesicles. Pure and mixed membrane growth kinetics were measured as previously reported.[44] The surface area changes were monitored at $\lambda^{ex} = 430$ nm and $\lambda^{em} = 586$ nm with the FRET donor/acceptor pair 1,2-dipalmitoyl-sn-glycero-3-phosphoethanolamine-N-(7-nitro-2-1,3-benzoxadiazol-4-yl) (NBD-PE) and N-(lissamine rhodamine B sulfonyl)-1,2-dihexadecanoyl-sn-glycero-3-phosphoethanolamine (LR-DhPE). The total mol % of the FRET-labeled lipids was 0.3 mol %, and the relative surface area changes were extrapolated using a calibration curve for fluorescence of known dye concentrations between 0.1 and 0.5 mol % (Figure S11C). 1% (v/v) TritonX-100 (1% (v/v)) was used to disrupt the signal to background levels and subsequently subtracted from each given concentration. To probe the dynamics between vesicles and micelles, Laurdan was dissolved in 100% ethanol as a 5 mM stock solution and added to vesicle solutions to 1% (v/v) prior to measurement. Fluorescence was monitored within 5−20 min, and after measurements, Triton X-100 was provided as 1% (v/v) to confirm the presence of micelles.

Lipid Flip-Flop Rates. The decay of a pH gradient across the membranes of vesicles was used to measure lipid flip-flop dynamics.[72] Vesicles were prepared as above with encapsulated 5 mM 8-hydroxypyrene-1,3,6-trisulfonic acid (HPTS), a pH-sensitive fluorophore, in 0.2 M Na^+-HEPES, pH 8.0 and mixed with 1:1 (v/v) 0.2 M Na^+-HEPES, pH 7.0. The Na^+ content of all buffers was adjusted with concentrated NaCl to 200 mM. All total lipid concentrations were kept at ≤2.5 mM to avoid artifacts from light scattering. Fluorescence was monitored continuously with $\lambda^{ex} = 460$ nm and $\lambda^{em} = 580$ nm for 2−200 points per second. The data was fit to a one-phase decay to get the rate (k).

Monomer Desorption Rates. HPTS was used to monitor the decay of a pH gradient across the membranes of reporter unilamellar POPC vesicles, as previously reported.[72,73] Since desorption kinetics are limiting for single chain lipids,[49] mixing donor single chain lipid vesicles with reporter POPC vesicles gives data indicative of monomer escape from the donor vesicles. Single-chain lipid vesicles (fatty acid and cyclophospholipid) were prepared as 10 mM total lipid, and POPC vesicles contained 5 mM HPTS in 0.2 M Na^+-HEPES, pH 8.0. The final concentrations of reporter and empty vesicles in the stopped-flow fluorimeter were ca. 1 and 2.5 mM, respectively. Measurements were with $\lambda^{ex} = 454$ nm and $\lambda^{em} = 515$ nm, with 10−200 points collected per second. To corroborate the HPTS-based measurements, the FRET donor/acceptor pairs NBD-PE and LR-DhPE (0.15 mol % each) were exploited and the FRET signals monitored with $\lambda^{ex} = 430$ nm and $\lambda^{em} = 586$ nm. Measurements were 2−20 points per second. For all measurements, an average of at least 5 different "shots" were taken into consideration. The raw data were fit to a one-phase decay $F_{(t)} = F_{(\infty)} + F_{(0)} \times e^{(-t/\tau)}$ to determine the experimental time constant $\tau = t_{obs}$, where $F_{(t)}$ indicates the fluorescence at given time point, $F_{(\infty)}$ is the fluorescence at the equilibrium point, and $F_{(0)}$ is the fluorescence at $t = 0$. Then, the $t_{1/2}$ was calculated as $\log_2(t_{obs})$, and k_{off} was calculated as $\frac{1}{t_{obs}}$, as reported

in Figure 4 and Figure S14. Fits gave an $R^2 > 0.8$ for 2 points per second measurements and $R^2 > 0.5$ for 20 points per second measurements.

Fluorescence Anisotropy. LUVs with a diameter of 100 nm were prepared with final total lipid concentration of 2.5 mM. Measurements were as previously reported.[44,74] Briefly, LUVs were mixed with 1,6-diphenyl-1,3,5-hexatriene (DPH) with a final concentration of 1% (v/v) from a concentrated ethanol stock of 1.25 mM. The LUVs were incubated for at least 1 h in the dark. Measurements were taken with fixed polarization angles of two separate detectors simultaneously, 0° (parallel) and 90° (perpendicular). Anisotropy was calculated as a unitless ratio with the formula: Anisotropy $= \frac{(I_= - I_\perp)}{(I_= - 2I_\perp)}$, where I is emission intensity at 430 nm ($\lambda^{ex} = 360$ nm) and $I_=$ is parallel and $I_\perp$ is perpendicular to the direction of polarization. The G-factor was calculated for every measurement for 10 s, and anisotropy measurements were performed for 60 s, with 1 data point per second. 60 s of measurement data were averaged and used as a single technical replicate. Then, at least four different replicates were averaged. Error bars indicate ± SD.

Permeability of Protocells. Solute permeability coefficients were determined using a previously established shrink−swell assay.[75] Briefly, unilamellar vesicles of 100 nm diameter with encapsulated 10 mM calcein were prepared as described above. Stopped-flow fluorescence kinetic measurements were taken with $\lambda^{ex} = 454$ nm and $\lambda^{em} = 515$ nm, with 2−200 points per second, depending on whether H_2O efflux or solute influx was monitored. For slow relaxation kinetics (>30 min), online fluorescence was used with quartz cuvettes. Fluorescence traces were fit as previously reported[75,76] to first-order, one-phase association kinetics where the solution to the differential equation $\frac{dN_s}{dt} = P_s \times A \times (C_{in} - C_{out})$ yields the permeability coefficient,[77] where $\frac{dN_s}{dt}$ stands for the derivative of the total amount of solute crossing the bilayer of LUVs over time, P_s indicates the permeability coefficient of the solute, A is the surface area of the LUVs, and C_{in} and C_{out} are the concentrations of solutes within and outside of the LUVs, respectively. Solutes were prepared either as 1.0 or 0.2 M stocks at the desired pH and were at 0.5 or 0.1 M final concentration. All buffers contained 1 mM EDTA. Buffer permeabilities were not relevant at the investigated time-scale.[17,44,78]

Protocell Stability. Cyclophospholipid-containing LUVs were prepared as above. However, after purification by size exclusion chromatography (SEC), the oligonucleotide-containing fractions (up to 4 earliest fractions, as depicted in Figure S16) were pooled, mixed with 25 mM Mg^{2+}-citrate, and incubated in the dark. At different time points, leakage was quantified by a second round of SEC equilibrated with 0.2 M Na^+-HEPES, pH 8.0, supplemented with lipid above the critical aggregate concentration (CAC), which was 20 mM for CPC10-based protocells and 2 mM for CPC18-based protocells. All oligonucleotides (Table S1) were encapsulated inside vesicles at a concentration of 25 μM in 0.2 M Na^+-HEPES, pH 8.0. Oligonucleotides were 10-mer polyA, 10-mer polyC, and 3-mer polyC DNA. All were labeled at the 5′-end with 6-FAM (fluorescein).

Template Directed Nonenzymatic Primer Extension. Nonenzymatic RNA primer extension followed previous reports.[79] Methanolic solution containing fatty acid, fatty alcohol, and cyclophospholipid was evaporated under a stream of N_2 to form a thin film on the walls of 2 mL glass vials and subsequently dried under vacuum overnight. The film was rehydrated with 0.25 M HEPES, pH 8.0, containing 50 μM 5′-FAM (fluorescein) labeled primer, 70 μM template, and 100 mM lipid. The vial was then rapidly vortexed and left tumbling overnight. The heterogeneous solution was extruded through a 100 nm polycarbonate membrane and then subjected to 20 cycles of freeze−thawing. Subsequently, $MgCl_2$ and sodium citrate were dissolved to achieve the final concentrations of 25 mM Mg^{2+} and 100 mM citrate, i.e., 1:4 Mg^{2+}:citrate, and incubated at room temperature for 2 h followed by purification by size-exclusion chromatography with sepharose 4B. Reactions were initiated by the addition of 10 mM guanosine-5′-phosphoro-(2-aminoimidazole) (2-AImpG). Aliquots were removed at different times for immediate

purification by size-exclusion chromatography. Tween-20 (0.1%, v/v) was then added to the fraction containing vesicles and vortexed. The nucleic acid was precipitated with cold isopropanol for at least 2 h at −20 °C, followed by two cycles of washing with cold isopropanol. Residual isopropanol was evaporated with a SpeedVac concentrator. The pellet was resuspended in water and quantified by fluorescence spectroscopy by exploiting the fluorescence arising from the 5′-FAM primer. Aliquots of equal fluorescence intensity were loaded onto a 20% urea polyacrylamide gel for separation. Visualization was performed with a Typhoon Laser-Scanner. The RNA oligonucleotides were the 12-mer primer 5′-(FAM)-AGUGAGUAACGG-3′ and 18-mer template 3′-UCACUCAUUGCCCCCCAA-5′ (Table S1). The oligonucleotides were synthesized using a K&A oligo-synthesizer. Activated guanosine was synthesized following a previous report.[80]

Dynamic Light Scattering and the Determination of Critical Vesicle Concentration. LUVs with a diameter of 100 nm were prepared with a final total lipid concentration of 2.5 mM. The measurements were collected with a Zetasizer Nano S (Malvern). The buffer was 0.2 M Na^+-HEPES, pH 8.0. The vesicles were prepared from methanol stocks, tumbled for 24 h, extruded to 100 nm, serially diluted in a 96-well plate (1:1 dilution, starting with 1 mM), and equilibrated for 24 h prior to measurement. The final volume in plastic (polypropylene) cuvette was 110 μM and measurements were collected at 23 °C. The attenuator was fixed at 10. The natural logarithm of the count rate was plotted, and inflection points where the slope changes were taken as the critical vesicle concentration (CVC) and critical micelle concentration (CMC).

ASSOCIATED CONTENT

Data Availability Statement

Data associated with this manuscript can be downloaded from Zenodo at https://zenodo.org/doi/10.5281/zenodo.10157375.

ⓈⒾ Supporting Information

The Supporting Information is available free of charge at https://pubs.acs.org/doi/10.1021/acsnano.3c07706.

Video of growth of 9:1 CPC18:oleate MLVs (MP4)
Video of division of 9:1 CPC18:oleate MLVs (MP4)
Video of division of 1:9 CPC18:oleate MLVs (MP4)
Structures of chemicals used in this study; growth of CPC18-based protocells in the presence and absence of Mg^{2+}-citrate; lack of growth of fatty acid protocells in the presence of Mg^{2+}-citrate; lack of growth when MLVs fed with same composition of LUVs; growth and division of MLVs fed with LUVs; division of oleate-rich MLVs fed with CPC18-rich LUVs; division of oleate-rich MLVs fed with pure CPC18 LUVs in the absence and presence of Mg^{2+}-citrate; calculations of hydrophobicity; effect of lipid composition on growth monitored by FRET; probing the micellar fraction of CPC18-based vesicles; lipid desorption rates; sugar permeability; encapsulation of oligonucleotides and small molecules; stability of cyclophospholipid-containing vesicles to pH and Mg^{2+}; growth and division of prebiotically plausible CPC10-based protocells in the absence and presence of Mg^{2+}-citrate; retention of small molecules and oligonucleotides; NMR spectra of CPC10 and CPC18; list of oligonucleotides used in this study (PDF)

AUTHOR INFORMATION

Corresponding Authors

Sheref S. Mansy − *Department of Cellular, Computational and Integrative Biology, University of Trento, 38123 Povo, Trentino, Italy; Department of Chemistry, University of Alberta, Edmonton, Alberta T6G 2G2, Canada;*

 orcid.org/0000-0003-2382-198X;
Email: sheref.mansy@ualberta.ca

Ramanarayanan Krishnamurthy − *Department of Chemistry, The Scripps Research Institute, La Jolla, California 92037, United States;* orcid.org/0000-0001-5238-610X; Email: rkrishna@scripps.edu

Jack W. Szostak − *Howard Hughes Medical Institute, Department of Chemistry, University of Chicago, Chicago, Illinois 60637, United States;* orcid.org/0000-0003-4131-1203; Email: jwszostak@uchicago.edu

Authors

Ö. Duhan Toparlak − *Department of Cellular, Computational and Integrative Biology, University of Trento, 38123 Povo, Trentino, Italy;* Present Address: Department of Chemistry, University of Oxford, 12 Mansfield Road, Oxford, OX1 3TA, UK

Lorenzo Sebastianelli − *Department of Chemistry, University of Alberta, Edmonton, Alberta T6G 2G2, Canada;* orcid.org/0000-0001-5242-6335

Veronica Egas Ortuno − *Department of Chemistry, The Scripps Research Institute, La Jolla, California 92037, United States*

Megha Karki − *Department of Chemistry, The Scripps Research Institute, La Jolla, California 92037, United States*

Yanfeng Xing − *Department of Biochemistry and Molecular Biology, University of Chicago, Chicago, Illinois 60637, United States*

Complete contact information is available at:
https://pubs.acs.org/10.1021/acsnano.3c07706

Author Contributions

Ö.D.T., L.S., V.E.O., M.K., and Y.X. performed the experiments. Ö.D.T., L.S., J.W.S., R.K., and S.S.M. conceptualized and designed the study. J.W.S., R.K., and S.S.M. supervised the project. Ö.D.T. wrote the original draft with S.S.M. All the authors edited the manuscript and approved the final version.

Notes

The authors declare no competing financial interest.

REFERENCES

(1) Horning, D. P.; Joyce, G. F. Amplification of RNA by an RNA polymerase ribozyme. *Proc. Natl. Acad. Sci. U. S. A.* **2016**, *113*, 9786−9791.

(2) Unrau, P. J.; Bartel, D. P. RNA-catalysed nucleotide synthesis. *Nature* **1998**, *395*, 260−263.

(3) Doudna, J. A.; Szostak, J. W. RNA-catalysed synthesis of complementary-strand RNA. *Nature* **1989**, *339*, 519−522.

(4) Attwater, J.; Raguram, A.; Morgunov, A. S.; Gianni, E.; Holliger, P. Ribozyme-catalysed RNA synthesis using triplet building blocks. *eLife* **2018**, *7*, e35255.

(5) Li, L.; et al. Enhanced nonenzymatic RNA copying with 2-aminoimidazole activated nucleotides. *J. Am. Chem. Soc.* **2017**, *139*, 1810−1813.

(6) Walton, T.; Zhang, W.; Li, L.; Tam, C. P.; Szostak, J. W. The mechanism of nonenzymatic template copying with imidazole-activated nucleotides. *Angew. Chem., Int. Ed.* **2019**, *58*, 10812.

(7) Hänle, E.; Richert, C. Enzyme-Free Replication with Two or Four Bases. *Angew. Chemie - Int. Ed.* **2018**, *57*, 8911−8915.

(8) Ichihashi, N.; Usui, K.; Kazuta, Y.; Sunami, T.; Matsuura, T.; Yomo, T. Darwinian evolution in a translation-coupled RNA replication system within a cell-like compartment. *Nat. Commun.* **2013**, *4*, 2494.

(9) Walde, P.; Umakoshi, H.; Stano, P.; Mavelli, F. Emergent properties arising from the assembly of amphiphiles. Artificial vesicle membranes as reaction promoters and regulators. *Chem. Commun.* **2014**, *50*, 10177−10197.

(10) Saha, R.; Verbanic, S.; Chen, I. A. Lipid vesicles chaperone an encapsulated RNA aptamer. *Nat. Commun.* **2018**, *9*, 2313.

(11) Peng, H.; Lelievre, A.; Landenfeld, K.; Müller, S.; Chen, I. A. Vesicle encapsulation stabilizes intermolecular association and structure formation of functional RNA and DNA. *Curr. Biol.* **2022**, *32*, 86−96.e6.

(12) Lai, Y. C.; Liu, Z.; Chen, I. A. Encapsulation of ribozymes inside model protocells leads to faster evolutionary adaptation. *Proc. Natl. Acad. Sci. U. S. A.* **2021**, *118*, e2025054118.

(13) Joyce, G. F.; Szostak, J. W. Protocells and RNA self-replication. *Cold Spring Harb. Perspect. Biol.* **2018**, *10*, a034801.

(14) Chen, I. A.; Roberts, R. W.; Szostak, J. W. The Emergence of Competition Between Model Protocells. *Science* **2004**, *305*, 1474−1476.

(15) Zhu, T. F.; Szostak, J. W. Coupled Growth and Division of Model Protocell Membranes. *J. Am. Chem. Soc.* **2009**, *131*, 5705−5713.

(16) Adamala, K.; Szostak, J. W. Competition between model protocells driven by an encapsulated catalyst. *Nat. Chem.* **2013**, *5*, 495−501.

(17) Toparlak, Ö. D.; Wang, A.; Mansy, S. S. Population-Level Membrane Diversity Triggers Growth and Division of Protocells. *JACS Au* **2021**, *1*, 560−568.

(18) Szostak, J. W. The eightfold path to non-enzymatic RNA replication. *J. Syst. Chem.* **2012**, *3*, 2.

(19) Szostak, J. W.; Bartel, D. P.; Luisi, P. L. Synthesizing life. *Nature* **2001**, *409*, 387.

(20) Deamer, D. W. Boundary structures are formed by organic components of the Murchison carbonaceaous chondrite. *Nature* **1985**, *317*, 792−794.

(21) Hargreaves, W. R.; Deamer, D. W. Liposomes from Ionic, Single-Chain Amphiphiles. *Biochemistry* **1978**, *17*, 3759−3768.

(22) Walde, P.; Wick, R.; Fresta, M.; Mangone, A.; Luisi, P. L. Autopoietic Self-Reproduction of Fatty Acid Vesicles. *J. Am. Chem. Soc.* **1994**, *116*, 11649−11654.

(23) Zhu, T. F.; Adamala, K.; Zhang, N.; Szostak, J. W. Photochemically driven redox chemistry induces protocell membrane pearling and division. *Proc. Natl. Acad. Sci. U. S. A.* **2012**, *109*, 9828.

(24) Berclaz, N.; Müller, M.; Walde, P.; Luisi, P. L. Growth and Transformation of Vesicles Studied by Ferritin Labeling and Cryotransmission Electron Microscopy. *J. Phys. Chem. B* **2001**, *105*, 1056−1064.

(25) Rushdi, A. I.; Simoneit, B. R. T. Lipid formation by aqueous Fischer−Tropsch-type synthesis over a temperature range of 100 to 400 °C. *Orig. Life Evol. Biosph.* **2001**, *31*, 103−118.

(26) Bonfio, C.; et al. Length-Selective Synthesis of Acylglycerol-Phosphates through Energy-Dissipative Cycling. *J. Am. Chem. Soc.* **2019**, *141*, 3934−3939.

(27) Chen, I. A.; Salehi-Ashtiani, K.; Szostak, J. W. RNA catalysis in model protocell vesicles. *J. Am. Chem. Soc.* **2005**, *127*, 13213−13219.

(28) Jin, L.; Kamat, N. P.; Jena, S.; Szostak, J. W. Fatty Acid/Phospholipid Blended Membranes: A Potential Intermediate State in Protocellular Evolution. *Small* **2018**, *14*, 1704077.

(29) Horning, D. P.; Samantha, B.; Tjhung, K. F.; Joyce, G. F. RNA-Catalyzed Polymerization and Replication of RNA. *Origin Life, Proc.* **2017**, *2017*, 4067.

(30) Wochner, A.; Attwater, J.; Coulson, A.; Holliger, P. Ribozyme-catalyzed transcription of an active ribozyme. *Science* **2011**, *332*, 209−212.

(31) Maurer, S. E.; Deamer, D. W.; Boncella, J. M.; Monnard, P. Chemical evolution of amphiphiles: glycerol monoacyl derivatives stabilize plausible prebiotic membranes. *Astrobiology* **2009**, *9*, 979−987.

(32) Sarkar, S.; Dagar, S.; Verma, A.; Rajamani, S. Compositional heterogeneity confers selective advantage to model protocellular membranes during the origins of cellular life. *Sci. Rep.* **2020**, *10*, 6−9.

(33) Budin, I.; Prywes, N.; Zhang, N.; Szostak, J. W. Chain-length heterogeneity allows for the assembly of fatty acid vesicles in dilute solutions. *Biophys. J.* **2014**, *107*, 1582−1590.

(34) Jordan, S. F.; et al. Promotion of protocell self-assembly from mixed amphiphiles at the origin of life. *Nat. Ecol. Evol.* **2019**, *3*, 1705−1714.

(35) Cornell, C. E.; et al. Prebiotic amino acids bind to and stabilize prebiotic fatty acid membranes. *Proc. Natl. Acad. Sci. U. S. A.* **2019**, *116*, 17239−17244.

(36) Black, R. A.; et al. Nucleobases bind to and stabilize aggregates of a prebiotic amphiphile, providing a viable mechanism for the emergence of protocells. *Proc. Natl. Acad. Sci. U. S. A.* **2013**, *110*, 13272−13276.

(37) Adamala, K.; Szostak, J. W. Nonenzymatic template-directed RNA synthesis inside model protocells. *Science* **2013**, *342*, 1098−1100.

(38) Tsuji, G.; Fujii, S.; Sunami, T.; Yomo, T. Sustainable proliferation of liposomes compatible with inner RNA replication. *Proc. Natl. Acad. Sci. U. S. A.* **2016**, *113*, 590−595.

(39) Terasawa, H.; Nishimura, K.; Suzuki, H.; Matsuura, T.; Yomo, T. Coupling of the fusion and budding of giant phospholipid vesicles containing macromolecules. *Proc. Natl. Acad. Sci. U. S. A.* **2012**, *109*, 5942−5947.

(40) Monnard, P.-A.; Walde, P. Current Ideas about Prebiological Compartmentalization. *Life* **2015**, *5*, 1239−1263.

(41) Ruiz-Mirazo, K.; Briones, C.; De La Escosura, A. Prebiotic systems chemistry: New perspectives for the origins of life. *Chem. Rev.* **2014**, *114*, 285−366.

(42) Toparlak, O. D.; Karki, M.; Egas Ortuno, V.; Krishnamurthy, R.; Mansy, S. S. Cyclophospholipids Increase Protocellular Stability to Metal Ions. *Small* **2020**, *16*, No. 1903381.

(43) Chen, I. A.; Szostak, J. W. A kinetic study of the growth of fatty acid vesicles. *Biophys. J.* **2004**, *87*, 988−998.

(44) Budin, I.; Szostak, J. W. Physical effects underlying the transition from primitive to modern cell membranes. *Proc. Natl. Acad. Sci. U. S. A.* **2011**, *108*, 5249−5254.

(45) Kindt, J. T.; Szostak, J. W.; Wang, A. Bulk self-assembly of giant, unilamellar vesicles. *ACS Nano* **2020**, *14*, 14627−14634.

(46) Urakami, N.; Sakuma, Y.; Chiba, T.; Imai, M. Vesicle deformation and division induced by flip-flops of lipid molecules. *Soft Matter* **2021**, *17*, 8434−8445.

(47) Piedrafita, G.; Monnard, P. A.; Mavelli, F.; Ruiz-Mirazo, K. Permeability-driven selection in a semi-empirical protocell model: The roots of prebiotic systems evolution. *Sci. Rep.* **2017**, *7*, 3141.

(48) Hamilton, J. A. Fatty acid transport: Difficult or easy? *J. Lipid Res.* **1998**, *39*, 467−481.

(49) McLean, L. R.; Phillips, M. C. Kinetics of Phosphatidylchohne and Lysophosphatidylcholine Exchange between Unilamellar Vesicles. *Biochemistry* **1984**, *23*, 4624−4630.

(50) Zhou, L.; Ding, D.; Szostak, J. W. The virtual circular genome model for primordial RNA replication. *RNA* **2021**, *27*, 1−11.

(51) Fahrenbach, A. C.; Giurgiu, C.; Tam, C. P.; Li, L.; Hongo, Y.; Aono, M.; Szostak, J. W. Common and Potentially Prebiotic Origin

for Precursor of Nucleotide Synthesis and Activation. *J. Am. Chem. Soc.* **2017**, *139*, 8780−8783.

(52) Li, L.; Prywes, N.; Tam, C. P.; O'Flaherty, D.; Lelyveld, V. S.; Izgu, E. C.; Pal, A.; Szostak, J. W. Enhanced Nonenzymatic RNA Copying with 2-Aminoimidazole Activated Nucleotides. *J. Am. Chem. Soc.* **2017**, *139*, 1810−1813.

(53) Patel, B. H.; Percivalle, C.; Ritson, D. J.; Duffy, C. D.; Sutherland, J. D. Common origins of RNA, protein and lipid precursors in a cyanosulfidic protometabolism. *Nat. Chem.* **2015**, *7*, 301−307.

(54) Nader, S.; Baccouche, A.; Connolly, F.; Abou-Ghanem, M.; Styler, S. A.; Lewis, J. D.; Pink, D.; Mansy, S. S. Model Atmospheric Aerosols Convert to Vesicles upon Entry into Aqueous Solution. *ACS Earth Space Chem.* **2023**, *7*, 252−259.

(55) Mayer, D. B.; Franosch, T.; Mast, C.; Braun, D. Thermophoresis beyond Local Thermodynamic Equilibrium. *Phys. Rev. Lett.* **2023**, *130*, No. 168202.

(56) Wachowius, F.; Attwater, J.; Holliger, P. Nucleic acids: Function and potential for abiogenesis. *Quart. Rev. Biophys.* **2017**, *50*, E4.

(57) Joyce, G. F. Bit by bit: The Darwinian basis of life. *PLoS Biol.* **2012**, *10*, e1001323.

(58) Czerniak, T.; Saenz, J. P. Lipid membranes modulate the activity of RNA through sequence-dependent interactions. *Proc. Natl. Acad. Sci. U. S. A.* **2022**, *119*, e2119235119.

(59) Paegel, B. M.; Joyce, G. F. Microfluidic compartmentalized directed evolution. *Chem. Biol.* **2010**, *17*, 717−724.

(60) Springsteen, G.; Yerabolu, J. R.; Nelson, J.; Rhea, C. J.; Krishnamurthy, R. Linked cycles of oxidative decarboxylation of glyoxylate as protometabolic analogs of the citric acid cycle. *Nat. Commun.* **2018**, *9*, 91.

(61) Stubbs, R. T.; Yadav, M.; Krishnamurthy, R.; Springsteen, G. A plausible metal-free ancestral analogue of the Krebs cycle composed entirely of α-ketoacids. *Nat. Chem.* **2020**, *12*, 1016−1022.

(62) Mariani, A.; Russell, D. A.; Javelle, T.; Sutherland, J. D. A Light-Releasable Potentially Prebiotic Nucleotide Activating Agent. *J. Am. Chem. Soc.* **2018**, *140*, 8657−8661.

(63) Gibard, C.; Bhowmik, S.; Karki, M.; Kim, E. K.; Krishnamurthy, R. Phosphorylation, oligomerization and self-assembly in water under potential prebiotic conditions. *Nat. Chem.* **2018**, *10*, 212−217.

(64) Liu, Z.; Wu, L.-F.; Xu, J.; Bonfio, C.; Russell, D. A.; Sutherland, J. D. Harnessing chemical energy for the activation and joining of prebiotic building blocks. *Nat. Chem.* **2020**, *12*, 1023.

(65) Foden, C. S.; Islam, S.; Fernandez-Garcia, C.; Maugeri, L.; Sheppard, T. D.; Powner, M. W. Prebiotic synthesis of cysteine peptides that catalyze peptide ligation in neutral water. *Science* **2020**, *370*, 865−869.

(66) Liu, L.; et al. Enzyme-free synthesis of natural phospholipids in water. *Nat. Chem.* **2020**, *12*, 1029−1034.

(67) Hardy, M. D.; et al. Self-reproducing catalyst drives repeated phospholipid synthesis and membrane growth. *Proc. Natl. Acad. Sci. U. S. A.* **2015**, *112*, 8187−8192.

(68) Ross, D.; Deamer, D. W. Dry/Wet Cycling and the Thermodynamics and Kinetics of Prebiotic Polymer Synthesis. *Life* **2016**, *6*, 28.

(69) Forsythe, J. G.; et al. Ester-Mediated Amide Bond Formation Driven by Wet-Dry Cycles: A Possible Path to Polypeptides on the Prebiotic Earth. *Angew. Chemie - Int. Ed.* **2015**, *54*, 9871−9875.

(70) Cohen, Z. R.; Cornell, C. E.; Catling, D. C.; Black, R. A.; Keller, S. L. Prebiotic Protocell Membranes Retain Encapsulated Contents during Flocculation, and Phospholipids Preserve Encapsulation during Dehydration. *Langmuir* **2022**, *38*, 1304−1310.

(71) Ortuno, V. E.; Pulletikurti, S.; Veena, K. S.; Krishnamurthy, R. Synthesis and Hydrolytic Stability of Cyclic Phosphatidic Acids: Implications for Synthetic- and Proto- cell Studies. *Chem. Commun.* **2022**, *58*, 6231−6234.

(72) Zhang, F.; Kamp, F.; Hamilton, J. A. Dissociation of long and very long chain fatty acids from phospholipid bilayers. *Biochemistry* **1996**, *35*, 16055−16060.

(73) McLean, L. R.; Phillips, M. C. Mechanism of Cholesterol and Phosphatidylcholine Exchange or Transfer between Unilamellar Vesicles. *Biochemistry* **1981**, *20*, 2893−2900.

(74) Zakim, D.; Daniels, C.; Noy, N. Rates of Hydration of Fatty Acids Bound to Unilamellar Vesicles of Phosphatidylcholine or to Albumin. *Biochemistry* **1985**, *24*, 3286−3292.

(75) Sacerdote, M. G.; Szostak, J. W. Semipermeable lipid bilayers exhibit diastereoselectivity favoring ribose. *Proc. Natl. Acad. Sci. U. S. A.* **2005**, *102*, 6004−6008.

(76) Perkins, R.; Vaida, V. Phenylalanine Increases Membrane Permeability. *J. Am. Chem. Soc.* **2017**, *139*, 14388.

(77) Chakrabarti, A. C.; Deamer, D. W. Permeability of lipid bilayers to amino acids and phosphate. *BBA - Biomembr.* **1992**, *1111*, 171−177.

(78) Mansy, S. S.; et al. Template-directed synthesis of a genetic polymer in a model protocell. *Nature* **2008**, *454*, 122−125.

(79) Jin, L.; Engelhart, A. E.; Adamala, K. P.; Szostak, J. W. Preparation, Purification, and Use of Fatty Acid-containing Liposomes. *J. Vis. Exp.* **2018**, 57324.

(80) Duzdevich, D.; Carr, C. E.; Ding, D.; Zhang, S. J.; Walton, T. S.; Szostak, J. W. Competition between bridged dinucleotides and activated mononucleotides determines the error frequency of nonenzymatic RNA primer extension. *Nucleic Acids Res.* **2021**, *49*, 3681−3691.